Current Applied Physics 16 (2016) 387–396

Contents lists available at ScienceDirect

Current Applied Physics

journal homepage: www.elsevier.com/locate/cap

Electrodeposition of 70-30 Cu–Ni nanocomposite coatings for enhanced mechanical and corrosion properties

Casey R. Thurber [a], Yahia H. Ahmad [b], Stephen F. Sanders [a], Amaal Al-Shenawa [c], Nandika D'Souza [c], Adel M.A. Mohamed [b, d], Teresa D. Golden [a, *]

[a] Department of Chemistry, University of North Texas, Denton, TX 76203, USA
[b] Center for Advanced Materials, Qatar University, PO Box 2713, Doha, Qatar
[c] Department of Mechanical and Energy Engineering, University of North Texas, Denton, TX 76207, USA
[d] Department of Metallurgical and Materials Engineering, Faculty of Petroleum and Mining Engineering, Suez University, Suez 4372, Egypt

ARTICLE INFO

Article history:
Received 18 September 2015
Received in revised form
16 December 2015
Accepted 24 December 2015
Available online 29 December 2015

Keywords:
Electrodeposition
Nanocomposites
Montmorillonite
Corrosion resistance
Cu–Ni alloys

ABSTRACT

A copper-nickel alloy (70:30 ratio) was electrochemically deposited and compared to a composite coating incorporating layered silicate platelets to obtain copper-nickel-montmorillonite (MMT). The composite coatings were electrochemically deposited from a citrate bath to investigate the effects of MMT on the corrosion and mechanical properties of the coatings. Incorporation of MMT into the Cu–Ni alloy films was not affected by the deposition parameters such as applied voltage and pH. Scanning electron microscopy and atomic absorption spectroscopy confirmed the successful incorporation of the MMT into the coatings. Longer term stability in the presence of corroding solutions was noted for the copper-nickel composite films. The Tafel calculations showed an increase in polarization resistance, R_p, from 190.7 kΩ·cm^2 for pure Cu–Ni to 314.3 kΩ·cm^2 for Cu–Ni-0.2% MMT after soaking the coatings in 3.5% NaCl at 25 °C for two weeks, which was consistent with the resistance increase measured by electrochemical impedance spectroscopy. Microhardness test results showed about a 25% increase in the hardness for the copper-nickel coatings incorporated with the layered silicate platelets versus the pure Cu–Ni coating.

© 2015 Elsevier B.V. All rights reserved.

1. Introduction

Composite coatings that slow the rate of corrosion at a reduced cost have been extensively studied over the past several years. Exposing films to an unfavorable environment accelerates the degradation of the film which can lead to multiple types of corrosion [1–4]. The rate of corrosion can be reduced using five general approaches which include the selection of materials, chemical inhibitors, changes in the environment, cathodic protection, or the addition of coatings [5]. Coatings can be produced by several different methods, and electrodeposition remains a prominent technique to produce novel materials for science and engineering applications because of low cost, convenience, ability to work at low temperatures and the ease of treatment to large and complex geometries [6,7].

One important route to increase the corrosion resistance of materials is the deposition of metallic alloys such as Zn–Ni, Ni–Mo, and Cu–Ni [8–10]. The alloyed coatings typically enhance the corrosion resistant properties but they possess mechanical properties that relate to the individual metals. Incorporating ceramic nanoparticles such as TiO_2, CeO_2, SiC, Al_2O_3, and ZrO_2 into the matrix of different coatings enhances the lifetime and performance of the coating [11–15]. However, addition of ceramics can lead to problems with delamination and brittleness producing shorter service times. Some silicates that have been used in composites are layered silicates [16–20]. Layered silicates have several advantageous properties such as a high surface area, chemical inertness, resistance to extreme temperatures, and resistance to pH changes [16–20]. MMT is the layered silicate being evaluated in this study, which is a platelet that measures ~1 nm in height and 1–2 microns in width [7]. One of the benefits of MMT over traditional spherical particles is its larger surface area, which helps to provide a more tortuous mean free path of corrosion. Also, MMT is a cationic clay with a negatively charged surface, which allows positively charged

* Corresponding author.
E-mail addresses: adel.mohamed@qu.edu.qa (A.M.A. Mohamed), tgolden@unt.edu (T.D. Golden).

http://dx.doi.org/10.1016/j.cap.2015.12.022
1567-1739/© 2015 Elsevier B.V. All rights reserved.

metal ions to be attracted to the surface, which helps to increase incorporation of the platelets into the metal matrix during the electrodeposition process. The addition/embedding of MMT into a pure nickel matrix was associated with an increase in hardness, adhesion, and corrosion resistance as shown in our previous work [4,21,22].

Alloys involving copper have been studied because of their machinability and resistance to biofouling [23]. Cu–Ni coatings used for several applications, such as decoration, microelectronics, corrosion resistant films, piping materials for the ship building industry, condensers, and heat exchangers have been analyzed over the years [24–31]. In the off-shore oil industry, two important properties, high corrosion resistance and hardness, are needed to extend the lifetime of coatings experiencing exposure to high stress and salt environments. Copper alloys are used in marine environments to defend against biofouling of materials by inhibiting microbial induced corrosion (MIC) [30–34]. Copper ions resist the growth of bacteria, viruses, fungi, algae and other microbes on the surface of the coating by reducing adhesion [29]. A popular alloy used is the 70-30 Cu–Ni (Alloy C71500) [31,35,36]. These alloys exhibit good corrosion resistance due to the growth of a protective layer at the surface of the coating [32,35]. The coating is comprised of a thin, strongly adherent inner Cu_2O layer acting as a barrier, in contact with the outer solution through a porous dense outer Cu(II) hydroxide/oxide layer [24].

In this work, Cu–Ni-MMT coatings were electrodeposited to improve corrosion and mechanical properties of the copper-nickel alloys. Citrate was utilized as the ligand to stabilize the electrolyte system. Citrate is a regularly used ligand for transition metal electrodeposition, and has been used effectively as a complexing agent for the deposition of Cu–Ni coatings [37–41]. There are pH restrictions when using citrate, due to an insoluble citrate complex forming and precipitating out of solution [30]. The distribution of citrate in the electrolyte as a function of composition, temperature and pH has been analyzed to try and stabilize the bath for longer periods of time [30]. It was observed that at the native pH of 4.1, the solution was unstable and a precipitate formed within a few days [30]. Solutions with citrate at pH 6.0 were found to be stable for several weeks with no precipitate formation [30]. For our study, the Cu–Ni citrate complex at pH 6.0 was used for the electrodeposition with MMT because of the proven long term stability.

2. Materials and methods

2.1. Materials and electrodeposition procedure

The layered silicate used in the coatings was MMT from Southern Clay Products. The MMT (0.05, 0.1, 0.2%) was stirred over a 24 h period to achieve exfoliated layered silicate platelets. 0.25 M trisodium citrate dihydrate (Fisher Scientific) was utilized as the ligand to stabilize the 70-30 Cu–Ni complex. 0.32 M nickel ammonium sulfate hexahydrate (Alfa Aesar) and 0.06 M copper sulfate pentahydrate (Fisher Scientific) were used as the metal salts. The prepared baths were adjusted to a pH of 6 with 2.0 M sodium hydroxide. The 1.8 cm^2 430 stainless steel substrates (Ted Pella) were polished with 600, 800, and 1000 grit silicon carbide paper, then with a 3 μm diamond suspension on a felt cloth. The polished electrodes were then sonicated in deionized water for 10 min and soaked in 5.0 M H_2SO_4 for 30 s before use.

An EG&G Princeton Applied Research Model 273A potentiostat/galvanostat was used for the electrodeposition, cyclic voltammetry, immersion test and Tafel analysis. The electrochemical system was made up of a three electrode system. The working, counter and reference electrodes were a stainless steel substrate, coiled chromel wire, and a saturated calomel reference (SCE), respectively. The solution was purged with N_2 for 15 min before deposition. Green et al. [37] reported that the stainless steel should be pre-treated prior to deposition of the copper-nickel coating to attain good adhesion. For the pretreatment, a Ni-MMT bath was used from a previous method to deposit a very thin layer [4]. The deposition conditions were 25 °C with E_{app} at −1.0 V until 30 coulombs of charge were obtained for the Cu–Ni films. The adhesion of the Cu–Ni and Cu–Ni-MMT coatings were measured on a DeFelsko, PosiTest AT-A (automatic) Pull-Off Adhesion Tester, and were all found to be greater than 75 N/mm^2. The Cu–Ni coatings were immersed in a 3.5% NaCl solution at 25 °C for 14 days while monitoring open circuit potential. The film thickness over different charge amounts for the coatings were measured using a Veeco Dektak 8 Stylus Profilometer.

2.2. Characterization studies

The zeta potential and particle size of the Cu–Ni plating solutions were measured using a Delsa Nano-C (Beckman-Coulter Instruments). The Cu–Ni solutions were allowed to adjust to 25 °C for 60 s using a peltier device in the instrument before data collection.

Atomic absorption spectroscopy (AAS) (Perkin Elmer Analyst 300) analysis was performed using the standard addition method to determine the optimal ratio of 70-30 Cu–Ni. X-ray diffraction (XRD) was used to analyze the crystal structure and particle size of the films. XRD (Siemens D-500 Diffractometer) was performed using the Cu Kα radiation $\lambda = 0.15406$ nm at 35 kV and 24 mA. The scans were obtained from 40 to 100° 2θ for the Cu–Ni coatings.

Scanning electron microscopy (SEM) and atomic force microscopy (AFM) were chosen to analyze the morphology and roughness of the electrodeposited coatings. The micrographs of the coatings were obtained using an Environmental FEI Quanta 200 scanning electron microscope with an Everhart Thornley detector. Energy dispersive spectroscopy (EDS) was used to determine the elemental composition of Cu–Ni and the layered silicate (Al and Si) in the composite coatings. A 3D surface topography of pure Cu–Ni and Cu–Ni-MMT coatings with various MMT concentrations was recorded by an AFM analyzer at a scan rate of 1.00 Hz and scan size 1.0 μm. AFM measurements were performed under ambient conditions using standard topography AC air (tapping mode in air).

The mechanical properties of the films was analyzed using microhardness and sheer strength testing. Microhardness was measured using a HMV-M Shimadzu microhardness testing machine model M3 (Kyoto, Japan). The applied load was 300 g for 10 s. For each test, three readings were done to represent the average value of microhardness. Sheer adhesion tests were measured using the XYZTEC instrument paired with a 2 mm wide knife. The knife was placed at 5 μm above the substrate-coating interface and moved 2 mm horizontally at a velocity 150 μm/s without hold time. The force to move as a function of distance was noted. The adhesive strength is the maximum recorded force divided by the area width of the knife X test distance. The test was repeated 6 times for each sample and the average of the values and standard deviation were calculated.

Corrosion behavior was analyzed by linear polarization techniques and electrochemical impedance spectroscopy (EIS) after a 2 week immersion in 3.5% NaCl at 25 °C. A three electrode electrochemical cell was used as the corrosion testing system which comprised of the working electrode films, two counter graphite rods, and a SCE as the reference electrode. A ±150 mV potential range was applied to the cell with a scan rate of 1 mV/s; the resulting current densities were then measured. EIS was performed in a three-electrode cell (where the working electrode is the coating layer) using a Bio-Logic Potentiostat/Galvanostat equipped with a software EC-Lab version 10.2. In the impedance

measurements, an input signal of 10 mV peak to peak was applied in the frequency domain of 0.1–10^5 Hz.

3. Results and discussion

3.1. Coating properties

3.1.1. Cyclic voltammetry and electrodeposition

Cyclic voltammetry (CV) was utilized to evaluate the effect of MMT on the reduction potential and the current response at the reduction potential. CV was run at scan rates of 5, 20, 50, and 100 mV/s. The CVs in Fig. 1 (run at 50 mV/s) for the Cu–Ni 70-30 baths with and without MMT, showed that there was no observed change in the reduction potential (−0.49 V) of copper or in the i_{pc} (cathodic peak current) when 0.05–0.2% MMT was loaded into the Cu–Ni plating bath. MMT did not change the reduction potential or current for copper deposition at the other scan rates also. The reduction peak for nickel is not observed due to hydrogen evolution. The anodic peak present at 0.32 V relates to the dissolution of the Cu–Ni complex. Varea et al. [26] discovered a large deviation in the amount of copper in Cu–Ni depositions by varying the voltage from −1.0 to −1.075 V, which lead to the conclusion that Cu deposition is diffusion-controlled and Ni deposition is charge transfer-controlled. The main difference in the voltammograms was that the MMT slightly pushed the hydrogen evolution more cathodic. This result revealed that the MMT platelets do not disrupt the redox potential for the deposition of the Cu–Ni.

Film thickness was measured over different charge amounts for pure Cu–Ni and Cu–Ni-MMT coatings to see if the MMT affected the deposition efficiency of the coatings. Table 1 shows coatings at 10 C, 20 C, and 30 C of charge for 70-30 Cu–Ni and 70-30 Cu–Ni-0.2% MMT. Graphical analysis revealed a linear increase in thickness for the pure Cu–Ni ($R^2 = 0.9985$) and Cu–Ni-MMT ($R^2 = 0.9979$) over the three charge amounts. The data showed that the growth of the film was the same for pure Cu–Ni and Cu–Ni incorporated with MMT, which meant MMT also had no effect on the deposition efficiency.

3.1.2. Particle size and zeta potential

The particle size and zeta potential (Table 2) of the Cu–Ni solutions were measured to test the stability of the plating solution (dispersion) after addition of MMT. The particle sizes of MMT in aqueous solution ranged from 440 to 540 nm for the three different concentrations. The particle size for the 70-30 Cu–Ni solutions increased as the concentration of MMT increased in the solution due to MMT platelet agglomeration. The metal ions in solution associate with the charged MMT platelets and promote agglomeration. This has been noted previously for nickel ions and MMT in solution [7]. Size of the MMT platelets can also be affected by the exfoliation method. In a previous study, a 0.5% MMT solution was prepared by stirring for 24 h giving a particle size of 591 nm and then the solution was ultrasonicated for one hour, which decreased the particle size to 231 nm [21]. The exfoliated MMT solutions of 0.05%, 0.1%, and 0.2% had zeta potentials around −39 mV. The exfoliated MMT is stable and able to disperse into the aqueous solution while the non-exfoliated MMT precipitates. For more stable suspensions, the ideal zeta potential would be a value more negative than −25 mV. The Cu–Ni-MMT plating solutions were around −19 to −20 mV. The adsorption of the Ni and Cu at the surface of the MMT platelet, moves the zeta potential towards a more positive value and helps to increase the particle size, which slightly decreases the electrostatic stabilization of the dispersion compared to pure MMT solution. However, the plating solutions still had enough stability for deposition purposes to stay suspended in solution throughout the deposition cycle producing viable coatings every 9 out of 10 times. Understanding the surface forces and tuning of the charges between the platelets and the electrode surface are essential for the incorporation of clay particles into the metal matrix during deposition [21]. To understand the complete mechanism for these metal composite films, further studies need to be examined.

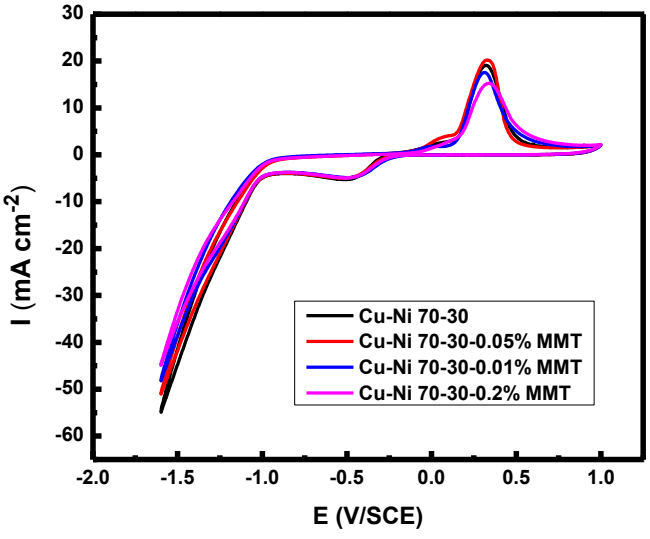

Fig. 1. Cyclic voltammograms of the 70-30 Cu–Ni films incorporated with MMT run at a scan rate of 50 mV/s.

3.1.3. X-ray diffraction

Copper and nickel both have a face centered cubic (fcc) crystal structure and are both similar in atomic size. The binary phase diagram for Cu–Ni shows complete solubility of copper into nickel in the liquid and solid state [42]. Hence, the Cu–Ni alloy is known as an isomorphous binary alloy, which means the two metals are completely soluble in one another and have one type of crystal structure. Varea et al. [26] showed that the (111) and (200) reflections shifted towards higher angles as the amount of copper decreased in the coating indicating an increase in the lattice parameter, which falls in agreement with Vegard's law.

XRD patterns were analyzed to evaluate the crystal structure and the particle size of the Cu–Ni and Cu–Ni-MMT composite coatings. Fig. 2A shows that deposition conditions favor a (111) preferred orientation. Only one major peak is present for the Cu–Ni alloy at a 2θ value of 43.6°, which is shifted between values for pure copper at 43.297° (PDF # 00-004-0836) and pure nickel at 44.508° (PDF # 00-004-0850). The peak present for the 70-30 Cu–Ni alloy at 43.6° corresponds to the preferred (111) orientation. Fig. 2B–D shows peak broadening of the (111) peak with the addition of MMT, which indicates a decrease in particle size and that the Cu–Ni structure is becoming amorphous. The particle size (L) for each film was calculated using the Scherrer equation:

$$B_r = k\lambda/L \cos\theta \quad (1)$$

The Gaussian peak fit method of $B_r^2 = B_o^2 - B_i^2$ was used to calculate the peak broadening, where B_o is the peak broadening of the coating and the B_i is the instrumental broadening calculated using a silicon standard. The proportionality constant k was assumed to be 1, $\lambda = 0.15406$ nm from the Cu Kα radiation, and θ is the position of the (111) peak. The calculated particle sizes listed in Table 3, showed the particle size decreased for the coatings incorporated with MMT. The decrease in particle size with the

Table 1
Thickness of the film versus total deposition charge to plate the film for 70-30 Cu–Ni and 70-30 Cu–Ni-0.2% MMT.

70-30 Cu–Ni Coatings		70-30 Cu–Ni-0.2% MMT coatings	
Deposition charge (C)	Film thickness (μm) (n = 3)	Deposition charge (C)	Film thickness (μm) (n = 3)
10	2.42 ± 0.03	10	2.42 ± 0.04
20	4.27 ± 0.04	20	4.26 ± 0.05
30	6.39 ± 0.07	30	6.42 ± 0.05

Table 2
Particle size and zeta potential for MMT and 70-30 Cu–Ni-MMT plating solutions.

Solutions	Particle size (nm) (n = 3)	Zeta potential (mV) (n = 3)
0.05% MMT	440 ± 15	−38.8 ± 0.5
0.1% MMT	500 ± 20	−39.2 ± 0.5
0.2% MMT	540 ± 10	−38.7 ± 0.4
70-30 Cu–Ni-0.05% MMT	2680 ± 80	−20.2 ± 0.7
70-30 Cu–Ni-0.1% MMT	2930 ± 70	−19.5 ± 0.6
70-30 Cu–Ni-0.2% MMT	3260 ± 60	−19.2 ± 0.7

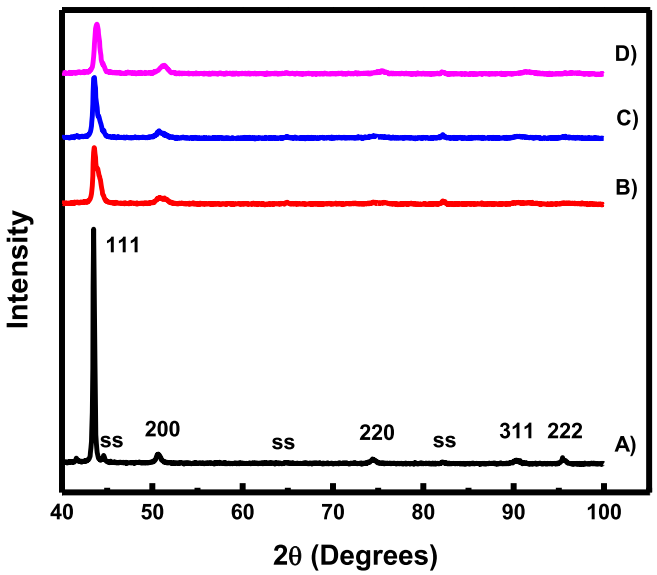

Fig. 2. X-ray diffraction patterns of: A) 70-30 Cu–Ni, B) 70-30 Cu–Ni-0.05% MMT, C) 70-30 Cu–Ni-0.1% MMT, and D) 70-30 Cu–Ni-0.2% MMT run from 40 to 100 2θ at a step size of 0.05° and dwell time of 1 s (ss – stainless steel substrate).

Table 3
Particle Sizes of the 70-30 Cu–Ni Coatings Calculated from the Scherrer Equation using X-ray Diffraction.

Coatings	Particle size (nm) (n = 3)
Cu–Ni (70-30)	62 ± 6
70-30 Cu–Ni – 0.05% MMT	16 ± 5
70-30 Cu–Ni – 0.1% MMT	15 ± 4
70-30 Cu–Ni – 0.2% MMT	15 ± 5

incorporation of MMT strengthens the grain refinement contribution to hardness, which explains the increase in the hardness of the coatings with embedded MMT.

3.1.4. Atomic absorption spectroscopy and energy dispersion spectroscopy

Atomic absorption spectroscopy was used to determine the composition of the Cu–Ni coatings. The analysis showed that the composition of 70-30 Cu–Ni was maintained during deposition at values of copper (71 ± 3%) and nickel (29 ± 3%). Also, EDS was performed to evaluate the Cu, Ni, Si, and Al composition of the coating. The Si and Al were evaluated because they are major components present in MMT. The EDS results in Table 4 showed that for the Cu–Ni 70-30 with 0.05% MMT, silicon content was 1.68% and aluminum was 1.09%. For the Cu–Ni 70-30 with 0.1% MMT, silicon content was 2.46% and aluminum was 1.50%. In the Cu–Ni 70-30 with 0.2%, the silicon content was 3.11% and 1.97% for aluminum, which confirmed the presence of MMT in the coatings. Also with the incorporation of MMT into the Cu–Ni matrix, the amount of Cu in the film slightly decreased and Ni slightly increased, indicating that MMT influenced a minor change in the Cu–Ni ratio during the deposition of the alloy. Previous data has shown that Ni adheres to the surface of MMT [7]. Nickel ions are in excess in the solution because of the deposition conditions and most of the copper is complexed with citrate. The slight increase in Ni concentration (and corresponding decrease in Cu) can be attributed to nickel ions adhering to the surface of MMT platelets as they are incorporated into the film.

3.1.5. Scanning electron microscopy and atomic force microscopy

Scanning electron microscopy was performed to examine the morphology of the prepared coatings. In Fig. 3, the pure Cu–Ni coating shows a tightly packed and uniform surface with well-defined grain boundaries. The pure Cu–Ni morphology also shows a corner like structure growth indicating a (111) preferred orientation which was observed in the XRD results. Fig. 3 also shows that with the incorporation of MMT into the Cu–Ni matrix, a smaller grain size was produced and the grain boundaries became less defined. With the increase in MMT concentration, additional small MMT platelets (red circles) can be observed on the surface, which were confirmed in the EDS results. The platelets at the surface of the coating may also contribute to the surface becoming slightly rougher in the AFM analysis.

In order to investigate the effect of incorporation of layered silicate into Cu–Ni metallic matrix on the surface roughness, AFM (Fig. 4) was performed on the surface of the coatings. The surface roughness of different samples were expressed by an average deviation parameter (R_a). The value of this parameter represents the average height of the surface irregularities in the direction perpendicular to the surface. The measured value of R_a of the pure 70-30 Cu–Ni was found to be 15.11 nm whereas the values in case of Cu–Ni-0.05% MMT, Cu–Ni-0.1% MMT and Cu–Ni-0.2% MMT are 17.25, 19.40 and 20.20 nm, respectively. The AFM results show that

Table 4
Energy Dispersive Spectroscopy of the 70-30 Cu–Ni Coatings incorporated with MMT.

Coatings	Copper (%)	Nickel (%)	Silicon (%)	Aluminum (%)
Cu–Ni (70-30)	68.96	31.04	–	–
70-30 Cu–Ni – 0.05% MMT	64.15	33.08	1.68	1.09
70-30 Cu–Ni – 0.1% MMT	63.91	32.13	2.46	1.50
70-30 Cu–Ni – 0.2% MMT	63.54	31.38	3.11	1.97

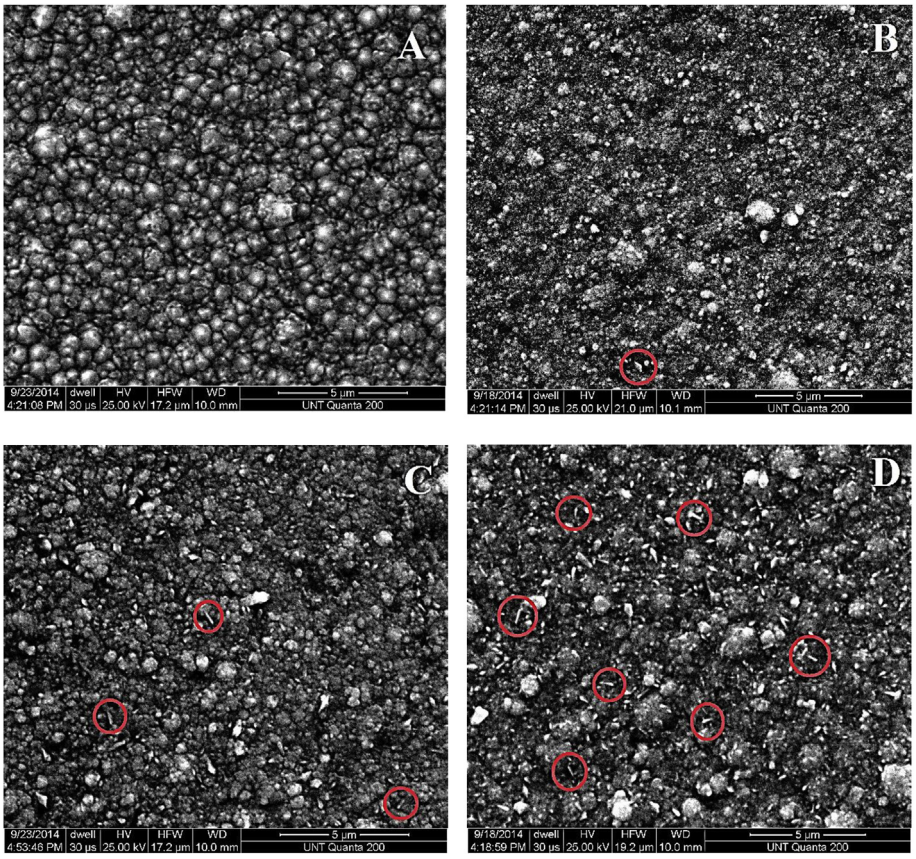

Fig. 3. SEM micrographs of: A) 70-30 Cu–Ni, B) 70-30 Cu–Ni-0.05% MMT, C) 70-30 Cu–Ni-0.1% MMT, and D) 70-30 Cu–Ni-0.2% MMT. Red circles indicate MMT platelets. (For interpretation of the references to colour in this figure legend, the reader is referred to the web version of this article.)

embedding MMT particles into the Cu–Ni metallic matrix resulted in a slight increase in the surface roughness of the coating.

3.1.6. Hardness

The hardness of metallic matrix composite is mainly governed by two factors; the microstructure of the metallic matrix and the amount of material embedded into the matrix. The microstructure of the metallic matrix is controlled by the parameters of the electrodeposition process including bath concentration of metallic ion, pH, applied voltage and the current density. Whereas, the amount of the material embedded into the matrix is dependent on its bath concentration, size of particles, solution pH and type of material. MMT has shown the ability to increase the hardness substantially in a pure nickel matrix [21].

The influence of MMT incorporation into the Cu–Ni matrix on microhardness was studied for the composite coatings. Table 5 represents the variation of the Cu–Ni-MMT film microhardness with the bath concentration of MMT. The microhardness of the composite coatings increased about 25% with the addition of MMT into the metallic layer. No statistical difference was observed between the different percentages of MMT embedded into the Cu–Ni matrix. This behavior may be attributed to the grain refinement caused by the embedding process which was evident in the particle size measurement from the XRD patterns.

3.1.7. Shear adhesion strength

The adhesion strength for the coatings are shown in Fig. 5. As can be seen, the shear adhesion strength of all the nanocomposite coatings exceeds that of the Cu–Ni matrix alone. The presence of the platelets provides enhanced resistance to the knife movement. The approximately 300% improvement in magnitudes for the 0.05% MMT point to the value of the presence of the platelets at low loadings. With increased MMT, the shear resistance decreases. This indicates that the increased amount of platelets in the coating lead to more substrate-platelet contact which would decrease the effective area of the matrix-substrate contact and lead to decreased adhesion strength. However, the adhesion strength is greater for all MMT loadings compared to the pure Cu–Ni film.

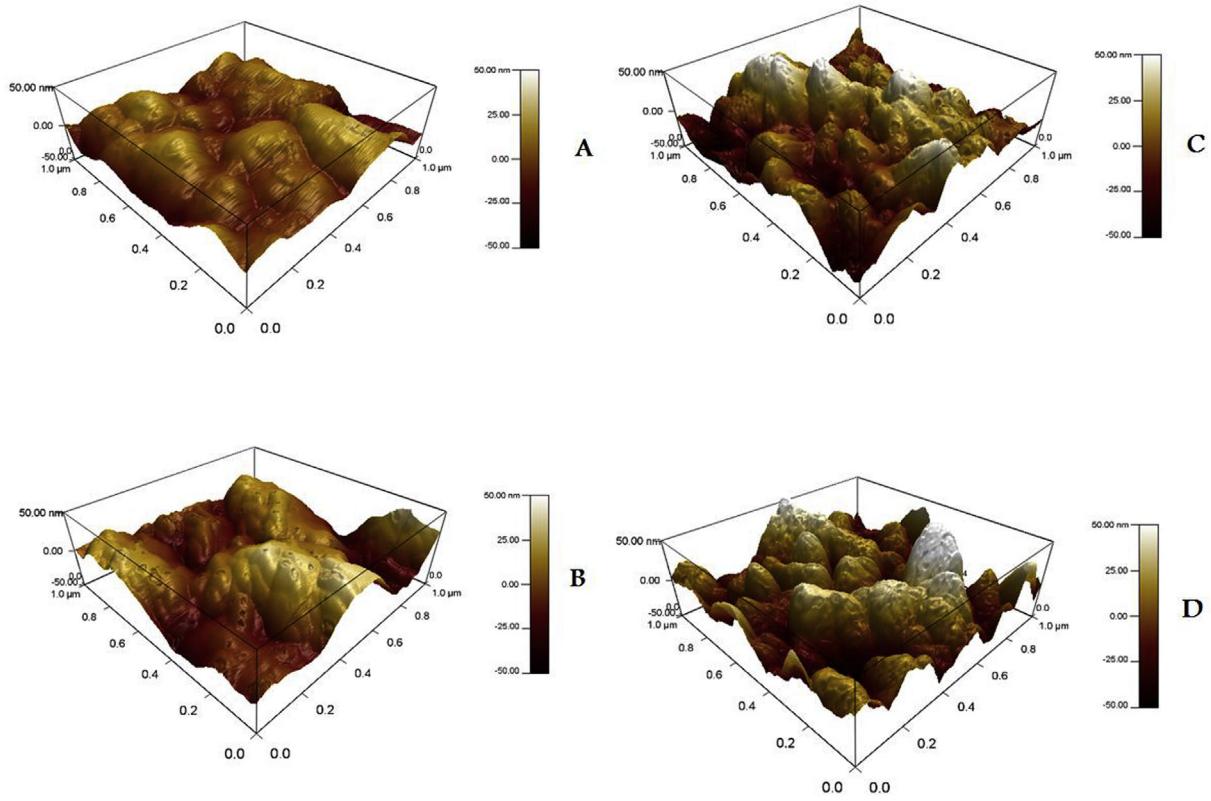

Fig. 4. AFM micrographs of: A) 70-30 Cu–Ni, B) 70-30 Cu–Ni-0.05% MMT, C) 70-30 Cu–Ni-0.1% MMT, and D) 70-30 Cu–Ni-0.2% MMT.

Table 5
Vickers Microhardness for the 70-30 Cu–Ni Coatings incorporated with MMT.

Coatings	Microhardness (HV) (n = 3)
Cu–Ni (70-30)	185 ± 5
70-30 Cu–Ni – 0.05% MMT	219 ± 10
70-30 Cu–Ni – 0.1% MMT	221 ± 10
70-30 Cu–Ni – 0.2% MMT	232 ± 8

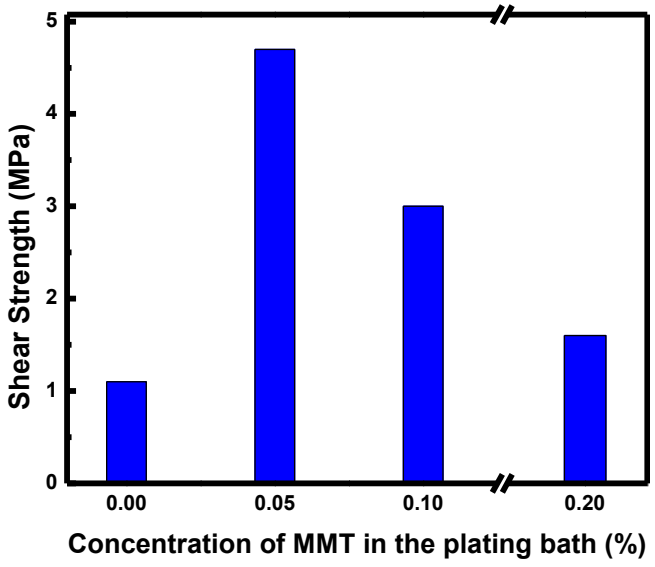

Fig. 5. The sheer adhesion strength of different coating layers versus the percentage of MMT in the plating solution.

3.2. Electrochemical properties

3.2.1. Immersion study

An immersion test of open circuit potential (OCP) vs. time was performed to evaluate the stability of the Cu–Ni coatings incorporated with and without MMT. Fig. 6 shows that in a 3.5% NaCl solution, the OCP of the pure Cu–Ni film shifted cathodically after five days followed by the Cu–Ni-0.05% MMT at seven days and the Cu–Ni-0.1% MMT at eleven days. The OCP of Cu–Ni-0.2% MMT

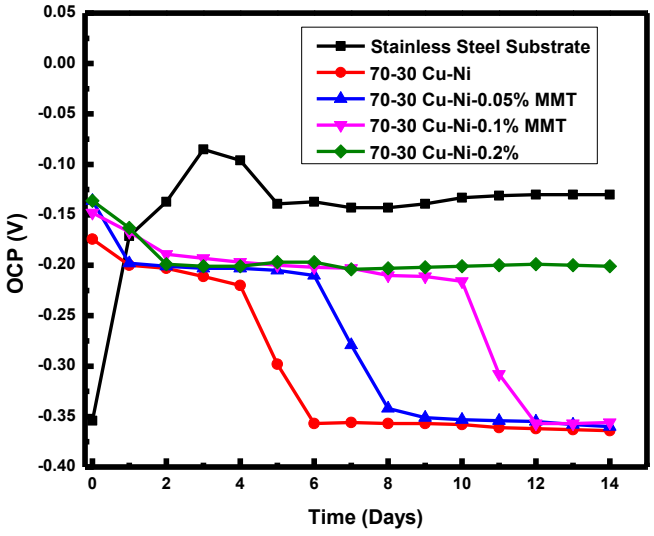

Fig. 6. Plot of the immersion test for the 70-30 Cu–Ni coatings with and without MMT measured by OCP vs. time for 2 weeks in a 3.5% NaCl solution.

stayed stable over the extended period of 14 days. The higher the amount of MMT in the coating, the more barrier type protection provided as seen in the OCP results. Incorporation of MMT helps slow the mean free path to corrosion. Al-Muhanna et al. [43] also observed a cathodic shift in OCP for 70-30 Cu–Ni in the first 10–15 days of study. Newly deposited Cu–Ni coatings have higher corrosion rates and then the rate drops as an oxide layer builds over time. The protective Cu_2O layer that forms on the surface of Cu–Ni during submersion is a p-type semiconductor with mobile cation vacancies as the main charge carriers. Nickel ions can diffuse into the layer interacting with vacancies to form neutral complexes [24,44,45]. Nickel has been found to segregate from the Cu–Ni alloy into the Cu_2O layer of Cu–Ni 70-30 with concentrations increasing up to 45% [24,44]. With nickel segregated into the outer layers of the film, it may help explain the cathodic shifts observed in the OCP with the pure Cu–Ni, Cu–Ni-0.05% MMT, and Cu–Ni-0.1% MMT because pure nickel is less noble than Cu–Ni, therefore it is observed at more negative potentials. This result shows that MMT slows the rate of nickel segregation into the Cu_2O layer and provides protection with grain refinement and surface area which lessens the mean free path of corrosion for the Cu–Ni matrix, which stabilizes and increases the corrosion resistance. The Cu–Ni-0.2% MMT film has definite enhanced stability for corrosion resistance.

3.2.2. Tafel analysis

The corrosion resistance of Cu–Ni and Cu–Ni-MMT composite coatings were evaluated using Tafel polarization, as seen in Fig. 7. The corrosion parameters were measured after immersing the prepared coatings for two weeks in a 3.5% NaCl solution at 25 °C. Table 6 lists the corrosion results for the Tafel plots. The E_{corr} values for the coatings matched the OCP values from day 14 of the immersion study. The i_{corr} values decreased, 1.24×10^{-6} to 5.60×10^{-7} A/cm^2, as the concentration of MMT increased in the Cu–Ni matrix. These values are similar to the values obtained by Varea et al. [26] for the i_{corr} of electrodeposited 70-30 Cu–Ni at 1.8×10^{-6} A/cm^2. The polarization resistance (R_p) was also calculated using the Stern-Geary equation:

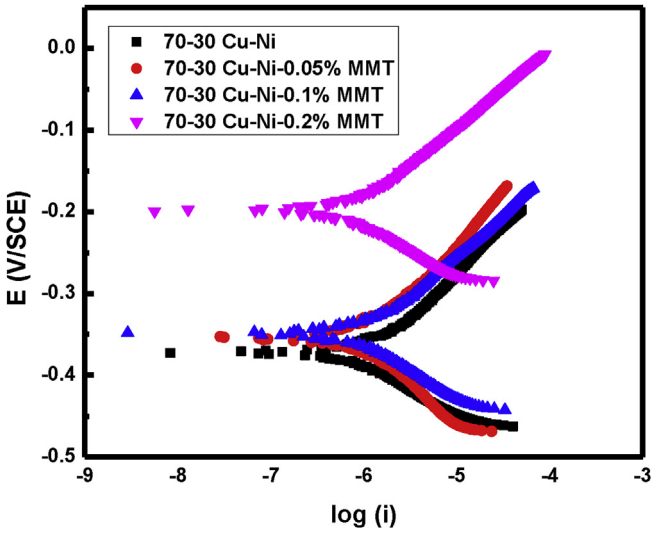

Fig. 7. Tafel plots for the 70-30 Cu–Ni coatings with and without MMT after being immersed in a 3.5% NaCl solution for 2 weeks.

Table 6
E_{corr}, I_{corr}, and polarization resistance (R_p) of 70-30 Cu–Ni Coatings incorporated with MMT.

Coatings	E_{corr} (V)	I_{corr} (A)	R_p (kΩ·cm^2)
70-30 Cu–Ni	−0.376	1.24×10^{-6}	190.7
70-30 Cu–Ni-0.05% MMT	−0.354	8.27×10^{-7}	208.1
70-30 Cu–Ni-0.1% MMT	−0.349	7.20×10^{-7}	239.7
70-30 Cu–Ni-0.2% MMT	−0.197	5.60×10^{-7}	314.3

$$Rp = \frac{\beta_a \, \beta_c}{2.303(\beta_a + \beta_c)} \left(\frac{1}{i_{corr}}\right) \quad (2)$$

β_a and β_c are the respective anodic and cathodic Tafel slopes. In Table 6, the R_p values of the 70-30 Cu–Ni incorporated with 0.05%, 0.1%, 0.2% MMT were 208.1, 239.7, and 314.3 kΩ·cm^2, respectively, compared to 190.7 kΩ·cm^2 in the case of the pure Cu–Ni film. The addition of MMT into the Cu–Ni matrix helped increase the corrosion resistance.

Before the active metal dissolution, the anodic part of the polarization curve relates to the creation of $CuCl^-$ adsorbed on the surface of the film. Due to copper dissolution, the current density rises with a rise in the potential by the direct creation of copper (I) chloride (3) or by Cu^+ dissolution to produce CuCl (4–5) [24,25,44]:

$$Cu + Cl^- \rightarrow CuCl + e^- \quad (3)$$

$$Cu \rightarrow Cu^+ + e^- \quad (4)$$

$$Cu^+ + Cl^- \rightarrow CuCl \quad (5)$$

The creation of $CuCl_2^-$ is observed at greater concentrations of chloride:

$$CuCl + Cl^- \rightarrow CuCl_2^- \quad (6)$$

The corrosion of copper alloys in chloride environments takes place through the cathodic reaction:

$$O_2 + 2H_2O + 4e^- \rightarrow 4OH^- \quad (7)$$

and the anodic reactions seen in Equations (3)–(6) [24,25,46]. The transport rate of $CuCl_2^-$ is slowed by an increase in pH close to the surface and begins to favor the creation of Cu_2O at the surface [24,25,46]:

$$2CuCl_2^- + 2H_2O \rightarrow Cu_2O + 2H^+ + 4Cl^- \quad (8)$$

Hence, the mass transport processes surrounding $CuCl_2^-$ and O_2 going back and forth from the corroding surface controls the corrosion mechanism [24,25].

A thick inner layer of Cu_2O and an outer layer of $Cu_2(OH)_3Cl$ have been confirmed to be the passivation components in chloride environments for Cu–Ni alloys, where the concentration of nickel does not exceed 40% [44]. Cu_2O is known to be the main constituent for good corrosion resistance because of its low electronic conductivity. The Cu_2O layer can incorporate different ions, such as nickel and iron because of the presence of vacancies [24,44,45]. The nickel products have been observed in the inner oxide layer by x-ray photoelectron spectroscopy [47]. The $Cu_2(OH)_3Cl$ layer forms by precipitation from the dissolution of Cu^{2+} after the formation of the Cu_2O layer [44,45]. The presence of the layered silicates for this mechanism helps with grain refinement and provides more surface area, thereby slowing the mean free path of corrosion.

3.2.3. Electrochemical impedance spectroscopy

The corrosion resistance of Cu–Ni and Cu–Ni-MMT composite coatings were also examined using EIS. Fig. 8 part A) and part B) are the Bode plots of 70-30 Cu–Ni and different Cu–Ni-MMT composite coatings after immersion in 3.5% NaCl solution for 14 days at 25 °C. The plots display two maximum phase lags, confirming the presence of two time constants corresponding to the corrosion/passivation processes taking place on the surface. The maximum value phase shift φ_{max} increases with increasing the amount of MMT imbedded into the Cu–Ni matrix which indicates more enhanced stability for the coating layer. The total resistance also increases as a result of embedding of MMT in the metallic matrix which confirms higher passivity of the composite film.

The experimental impedance data were simulated using different models and the best fit was obtained when using the equivalent circuit model shown in the inset for Fig. 9. The fitting values showed good agreement between the theoretical and measured values when a frequency dependent constant phase element (Q) was used instead of pure capacitor. The impedance related to the capacitance of this constant phase element is a combination of properties related to the surface and the electroactive species and it can be expressed as:

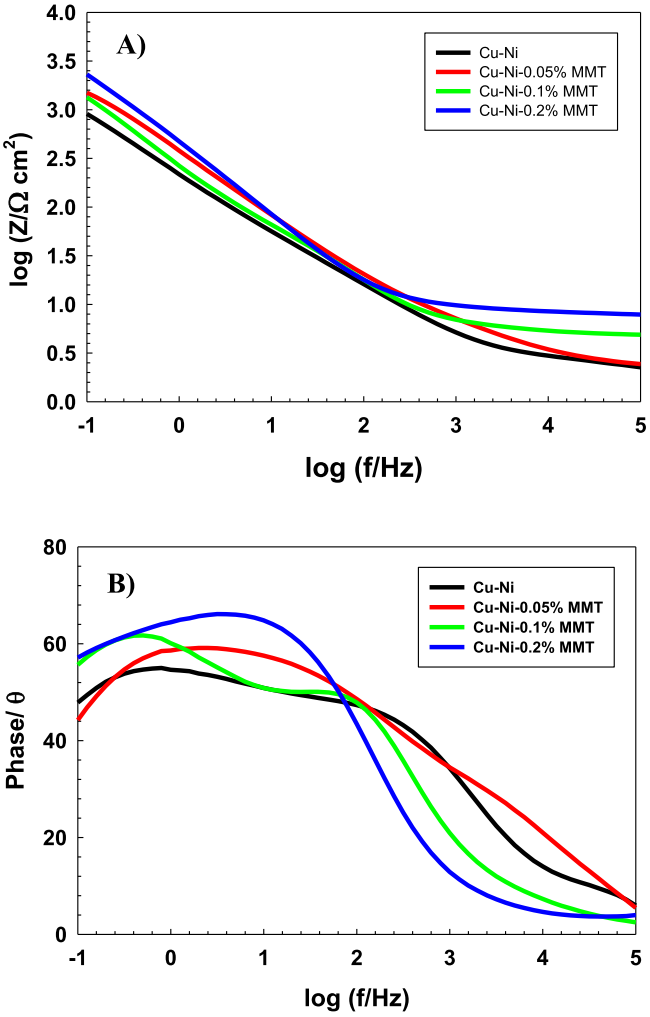

Fig. 8. A) Bode impedance plot and B) Bode phase plot of pure 70-30 Cu–Ni and different 70-30 Cu–Ni-MMT composite coatings after 2 weeks of immersion in a 3.5% NaCl solution.

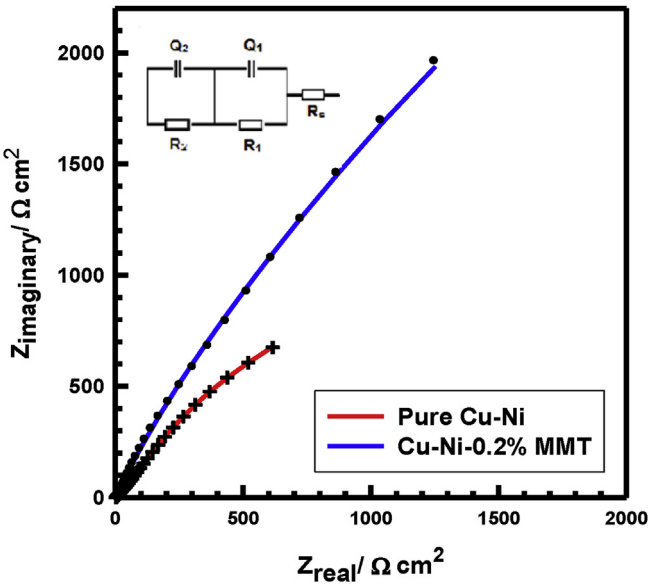

Fig. 9. Nyquist impedance plots of pure 70-30 Cu–Ni and 70-30 Cu–Ni-0.2% MMT after being immersed in a 3.5% NaCl solution for 2 weeks and the equivalent circuit representing the electrode/electrolyte interface for the electrodeposited layer in the saline solution.

$$Z_{CPE} = Y_0^{-1}(j\omega)^{-\alpha} \tag{9}$$

where Y_0 is the frequency independent real constant of the constant phase element which is identical to the ideal capacitance at $\omega = 1$, where ω being the angular frequency ($\omega = 2\pi f$), $j = \sqrt{-1}$ and α is an adjustable empirical exponent, its value ranges from 0 to 1.0 (pure capacitive behavior and perfectly smooth surface) and its value is 0.5 for a porous electrode.

The equivalent circuit model used to fit the measured impedance values consists of two circuits R_1Q_1 and R_2Q_2 parallel combinations and the two circuits are in series with the solution resistance (R_s). Generally, the passive films comprise two layers: a thin barrier layer which is usually compact and crystalline and an outer layer which has usually higher thickness and porous. Accordingly, Q_1 is related to the contribution from outer layer capacitance and Q_2 of the barrier inner layer, whereas R_1 and R_2 are the resistances of the outer and inner layers constituting the passive layer, respectively.

According to this model, the total capacitance of the film can be expressed as:

$$C^{-1} = Q_1^{-1} + Q_2^{-1} \tag{10}$$

This circuit has several structures, one of them is the Voight model, where impedance can be expressed as:

$$Z(\omega) = R_0 + \frac{R_1}{1 + R_1Q_1(j\omega)^{\alpha_1}} + \frac{R_2}{1 + R_2Q_2(j\omega)^{\alpha_2}} \quad \text{where } 0 \leq \alpha_1,\ \alpha_2 \leq 1 \tag{11}$$

Nyquist plots of pure Cu–Ni and Cu–Ni-0.2% MMT composite coatings after 14 days immersion in 3.5% NaCl at 25 °C are represented in Fig. 9. The diameter of the depressed uncompleted semi circles is larger in case of Cu–Ni-MMT compared to pure Cu–Ni, which indicates increased stability of the passive film in the case of Cu–Ni-MMT compared to that of pure Cu–Ni. The equivalent circuit parameters of the fitting procedure are presented in Table 7. The calculated parameters show higher resistance for the inner layer in

Table 7
The equivalent circuit parameters of pure 70-30 Cu–Ni and Cu–Ni-MMT composite coatings after 2 weeks immersion in 3.5% NaCl solution.

Coatings	R_s (Ω cm^2)	R_1 (Ω cm^2)	Q_1 (Ω^{-1} s$^{\alpha}$ cm^{-2})	α_1	R_2 (kΩ cm^2)	Q_2 (Ω^{-1} s$^{\alpha}$ cm^{-2})	α_2
70-30 Cu–Ni	2.25	49.78	2.95×10^{-3}	0.56	2.87	1336×10^{-6}	0.73
70-30 Cu–Ni-0.05% MMT	0.78	5.45	6.20×10^{-3}	0.75	3.02	954×10^{-6}	0.75
70-30 Cu–Ni-0.1% MMT	5.01	54.0	1.26×10^{-3}	0.68	4.92	709×10^{-6}	0.80
70-30 Cu–Ni-0.2% MMT	8.32	95.20	2.33×10^{-6}	0.99	13.77	583×10^{-6}	0.76

case of Cu–Ni-MMT composite coating compared to that of pure Cu–Ni, this resistance increases as the MMT content in the metallic matrix increases which is consistent with the data obtained from potentiodynamic polarization, and also confirms that embedding of layered silicate particles into Cu–Ni metallic matrix increases its corrosion resistance.

4. Conclusions

With successful incorporation of MMT into the Cu–Ni matrix, the corrosion and mechanical properties were improved over the pure Cu–Ni alloy coating, as shown with Tafel analysis, EIS, and mechanical testing. Electrochemical plating bath conditions were found to control the composition of copper and nickel during electrodeposition, as seen in the AAS analysis. Cu–Ni-0.2% MMT proved to have the best corrosion resistance and hardness. These films may prove to be beneficial as corrosion resistant coatings for the marine environment.

Acknowledgments

This work was made possible by NPRP Grant 4-306-2-111 from the Qatar National Research Fund (a Member of The Qatar Foundation). The statements made herein are solely the responsibility of the authors. The authors acknowledge the Center for Advanced Research and Technology (CART) at the University of North Texas.

References

[1] W.Z. Friend, Corrosion of Nickel and Nickel-base Alloys, Willey-Interscience, New York, 1980.
[2] Y.Y. Chang, D.Y. Wang, Corrosion behavior of electroless nickel-coated AISI 304 stainless steel enhanced by titanium ion implantation, Surf. Coat. Tech. 200 (2005) 2187–2191.
[3] P.T. Tang, Pulse reversal plating of nickel alloys, Inst. Metal Finish. 85 (2007) 51–56.
[4] J. Tientong, C.R. Thurber, N. D'Souza, A.M.A. Mohamed, T.D. Golden, Influence of bath composition at acidic pH on electrodeposition of nickel-layered silicate nanocomposites for corrosion protection, Int. J. Electrochem 2013 (2013) 1–8.
[5] Painting: New Construction and Maintenance, U.S Army Corps of Engineers, 2-1 1995. EM 1110-2–3400.
[6] A.J. Bard, L.R. Faulkner, Electrochemical Methods: Fundamentals and Applications, 2000. New York.
[7] R.A. Horch, T.D. Golden, N.A. D'Souza, L. Riester, Electrodeposition of nickel/montmorillonite layered silicate nanocomposite thin films, Chem. Mater. 14 (2002) 3531–3538.
[8] H.A. Conrad, J.R. Corbett, T.D. Golden, Electrochemical deposition of γ-phase zinc-nickel alloys from alkaline solution, J. Electrochem. Soc. 159 (2012) C29–C32.
[9] Y.H. Ahmad, A.M.A. Mohamed, T.D. Golden, N. D'Souza, Electrodeposition of nanocrystalline Ni-Mo alloys from alkaline glycinate solutions, Int. J. Electrochem. Sci. 9 (2014) 6438–6450.
[10] S.J. Yuan, S.O. Pehkonen, Surface characterization and corrosion behavior of 70/30 Cu–Ni alloy in pristine and sulfide-containing simulated seawater, Corros. Sci. 49 (2007) 1276–1304.
[11] D.E. Rusu, P. Cojocaru, L. Magagnin, C. Gheorghies, G. Carac, Study of Ni-TiO_2 nanocomposite coating prepared by electrochemical deposition, J. Optoelectron Adv. M. 12 (2010) 2419–2422.
[12] R. Sen, S. Das, K. Das, Synthesis and properties of pulse electrodeposited Ni-CeO_2 nanocomposite, Metall. Mater. Trans. A 43A (2012) 3809–3823.
[13] M.R. Vaezi, S.K. Sadrnezhaad, L. Nikzad, Electrodeposition of Ni–SiC nanocomposite coatings and evaluation of wear and corrosion resistance and electroplating characteristics, Colloids Surf. A 315 (2008) 176–182.
[14] L.M. Chang, J.H. Liu, R.J. Zhang, Corrosion behaviour of electrodeposited Ni/Al_2O_3 composite coating covered with a NaCl salt film at 800 °C, Mater. Corros. 62 (2011) 920–925.
[15] Y.H. Ahmad, A.M.A. Mohamed, Electrodeposition of nanostructured nickel-ceramic composite coatings: a review, Int. J. Electrochem. Sci. 9 (2014) 1942.
[16] L. Sahu, N.A. D'Souza, Interfacial effects in montmorillonite filled polyester thin films, Open Macromol. J. 6 (2012) 28–32.
[17] E. Ogunsona, S. Ogbomo, M. Nar, N.A. D'Souza, Thermal and mechanical effects in polystyrene-montmorillonite nanocomposite foams, Cell. Polym. 30 (2011) 79–93.
[18] M.C. Richardson, J. Kim, D. Ho, C.R. Snyder, N.A. D'Souza, G.A. Holmes, Organofunctionalized montmorillonite/epoxy nanocomposites: the effect of interlayer cation distribution on mechanical properties, Polym. Compos. 32 (2011) 67–78.
[19] Q. Wang, N.A. D'Souza, T.D. Golden, Ceramic montmorillonite nanocomposites by electrochemical synthesis, App. Clay Sci. 42 (2008) 310–317.
[20] A.Q. Wang, N.A. D'Souza, T.D. Golden, Electrosynthesis of nanocrystalline cerium oxide/layered silicate powders, J. Mater. Chem. 16 (2006) 481–488.
[21] J. Tientong, Y.H. Ahmad, M. Nar, N. D'Souza, A.M.A. Mohamed, T.D. Golden, Improved mechanical and corrosion properties of nickel composite coatings by incorporation of layered silicates, Mater. Chem. Phys. 145 (2014) 44–50.
[22] Y.H. Ahmad, J. Tientong, N. D'Souza, T.D. Golden, A.M.A. Mohamed, Salt water corrosion resistance of electrodeposited Ni-layered silicate nanocomposite coatings from Watts' type Solution, Surf. Coat. Tech. 242 (2014) 170–176.
[23] S. Mohan, N. Rajasekaren, Influence of electrolyte pH on composition, corrosion properties and surface morphology of electrodeposited Cu-Ni alloy, Surf. Eng. 7 (2011) 519–523.
[24] M. Metikos-Hukovic, I. Skugor, Z. Grubac, R. Babic, Complexities of corrosion behaviour of copper–nickel alloys under liquid impingement conditions in saline water, Electrochim. Acta 55 (2010) 3123–3129.
[25] M. Metikos-Hukovic, R. Babic, I. Skugor, Z. Grubac, Copper–nickel alloys modified with thin surface films: corrosion behaviour in the presence of chloride ions, Corr. Sci. 53 (2011) 347–352.
[26] A. Varea, E. Pellicer, S. Pané, B.J. Nelson, S. Suriñach, M.D. Baró, J. Sort, Mechanical properties and corrosion behavior of nanostructured Cu-rich CuNi electrodeposited films, Int. J. Electrochem. Sci. 7 (2012) 1288–1302.
[27] T.S.N. Baskaran, S. Narayanan, A. Stephen, Pulsed electrodeposition of nanocrystalline Cu–Ni alloy films and evaluation of their characteristic properties, Mater. Lett. 60 (2006) 1990–1995.
[28] M. Alper, H. Kockar, M. Safak, M.C. Baykul, Comparison of Ni-Cu alloy films electrodeposited at low and high pH levels, J. Alloys Compd. 453 (2008) 15–19.
[29] E. Pellicer, A. Varea, S. Pane, K.M. Sivaraman, B.J. Nelson, S. Surinach, M.D. Baro, J. Sort, A comparison between fine-grained and nanocrystalline electrodeposited Cu–Ni films. Insights on mechanical and corrosion performance, Surf. Coat. Tech. 205 (2011) 5285–5293.
[30] W. Schleich, Typical failures of CuNi 90/10 seawater tubing systems and how to avoid them, Eurocorr 2004 (2004) 1–10.
[31] B.E.T. Bautista, M.L. Carvalho, A. Seyeux, S. Zanna, P. Cristiani, B. Tribollet, P. Marcus, I. Frateur, Effect of protein adsorption on the corrosion behavior of 70Cu-30Ni alloy in artificial seawater, Bioelectrochemistry 97 (2014) 34–42.
[32] R.S. Gonçalves, D.S. Azambuja, A.M.S. Lucho, M.P. Reche, A.M. Schmidt, Electrochemical studies of copper, nickel, and a Cu55/Ni45 alloy in aqueous sodium acetate, Mater. Res. 4 (2001) 97–101.
[33] W.A. Badawy, K.M. Ismail, A.M. Fathi, The influence of the copper/nickel ratio on the electrochemical behavior of Cu-Ni alloys in acidic sulfate solutions, J. Alloys Compd. 484 (2009) 365–370.
[34] V.A.R. Boyapati, C.K. Kanukula, Corrosion inhibition of Cu-Ni (90/10) alloy in seawater and sulphide-polluted seawater environments by 1, 2, 3-Benzotriazole, ISRN Corros. 2013 (2013) 1–22.
[35] W. Schleich, R. Feser, G. Schmitt, S. Haarmann, K. Schnier, Effect of Seawater Chlorination on the Erosion Corrosion Behaviour of CuNi 90/10, Eurocorr, CDA Publication, 2007, pp. 1–14.
[36] K. Al-Muhanna, K. Habib, Marine bio-fouling of different alloys exposed to continuous flowing fresh seawater by electrochemical impedance spectroscopy, J. Saudi Chem. Soc. (2012) 1–6.
[37] T.A. Green, A.E. Russell, S.J. Roy, The development of a stable citrate electrolyte for the electrodeposition of copper-nickel alloys, J. Electrochem. Soc. 145 (1998) 875–881.
[38] S. Rode, C. Henninot, C. Vallières, M. Matlosz, Complexation chemistry in copper plating from citrate baths, J. Electrochem. Soc. 151 (2004) C405–C411.
[39] E.J. Podlaha, C. Bonhôte, D. Landolt, A mathematically model and experimental study of the electrodeposition of Ni-Cu alloys from complexing electrolytes, Electrochim. Acta 39 (1994) 2649–2657.

[40] S. Rode, C. Henninot, M. Matlosz, Complexation chemistry in nickel and copper-nickel alloy plating from citrate baths, J. Electrochem. Soc. 152 (2005) C248–C254.
[41] R.Y. Ying, P.K. Ng, Z. Mao, R.E. White, Electrodeposition of Cu-Ni alloys from citrate solutions on a rotating disk electrode, J. Electrochem. Soc. 135 (1988) 2964–2971.
[42] A. Karimbeigi, A. Zakeri, A. Sadighzadeh, Effect of composition and milling time on the synthesis of nanostructured Ni-Cu alloys by mechanical alloying method, Iran. J. Mater. Sci. Eng. 10 (2013) 27–31.
[43] K. Al-Muhanna, K. Habib, Corrosion behavior of different alloys exposed to continuous flowing seawater by electrochemical impedance spectroscopy (EIS), Desalin 250 (2010) 404–407.
[44] I. Milosev, M. Metikos-Hukovic, The behaviour of Cu-xNi (x = 10 to 40 wt%) alloys in alkaline solutions containing chloride ions, Electrochim. Acta 42 (1997) 1537–1548.
[45] A.L. Ma, S.L. Jiang, Y.G. Zheng, W. Ke, Corrosion product film formed on the 90/10 copper–nickel tube in natural seawater: composition/structure and formation mechanism, Corros. Sci. 91 (2015) 245–261.
[46] W.A. Badaway, K.M. Ismail, A.M. Fathi, Effect of Ni content on the corrosion behavior of Cu-Ni alloys in neutral chloride solutions, Electrochim. Acta 50 (2005) 3603–3608.
[47] B.V. Appa Roa, K.C. Kumar, N.Y. Hebalker, X-ray photoelectron spectroscopy depth-profiling analysis of surface films formed on Cu–Ni (90/10) alloy in seawater in the absence and presence of 1,2,3-benzotriazole, Thin Solid Films 556 (2014) 337–344.